BASIC PHYSICAL PROPERTIES OF POLYCRYSTALLINE MgB_2 PELLETS AND WIRES.

P. C. Canfield, S. L. Bud'ko, D. K. Finnemore, G. Lapertot, C. Petrovic, C. E. Cunningham, and V. G. Kogan

Ames Laboratory and Department of Physics and Astronomy, Iowa State University, Ames, IA 50011, USA

M-H. Jung and A. H. Lacerda

National High Magnetic Field Laboratory - Pulse Facility Los Alamos National Laboratory, MS E536 Los Alamos, NM 87545, USA

The discovery of superconductivity in MgB_2 [1] has lead to an intensive examination of the basic properties of this simple binary compound. Within half year of the January 2001 announcement a wealth of information about the synthesis and basic properties of powders, wires and films of MgB_2 has been submitted for publication.

In this paper we will review the synthesis and characterization of MgB_2. We will start with an overview of how to produce MgB_2 in a variety of forms via exposure of elemental B to Mg vapor. This will be followed by a review of the results of measurements on the samples made with isotopically pure ^{11}B and ^{10}B. In thermodynamic as well as transport properties there is a

clear isotope shift of approximately 1 K, a value that is consistent with phonon mediated, BCS superconductivity. We will then present the results of measurements on wire segments, as well as sintered pellets that delineate the basic properties of MgB_2 and allow for estimates of normal state as well as superconducting length scales. Finally we will discuss recent results that indicate that MgB_2 may well have significant anisotropies associated with the superconducting state.

Given that many of the researchers active in this rapidly growing field will be contributing to this volume, in this paper we will primarily review the work that has been done by the Ames Laboratory group and collaborators. This is not meant to be a review of the literature as a whole, but a summary of our own contributions to the first months of this field.

SYNTHESIS OF MgB_2 PELLETS, WIRE SEGMENTS AND THIN FILMS

The binary phase diagram for Mg – B is shown in Figure 1. MgB_2 is shown as a line compound that decomposed near 1500°C when it is in equilibrium with Mg vapor. The lack of an exposed liquidus – solidus line for MgB_2 indicates that MgB_2 is unlikely to be grown out of a binary melt.

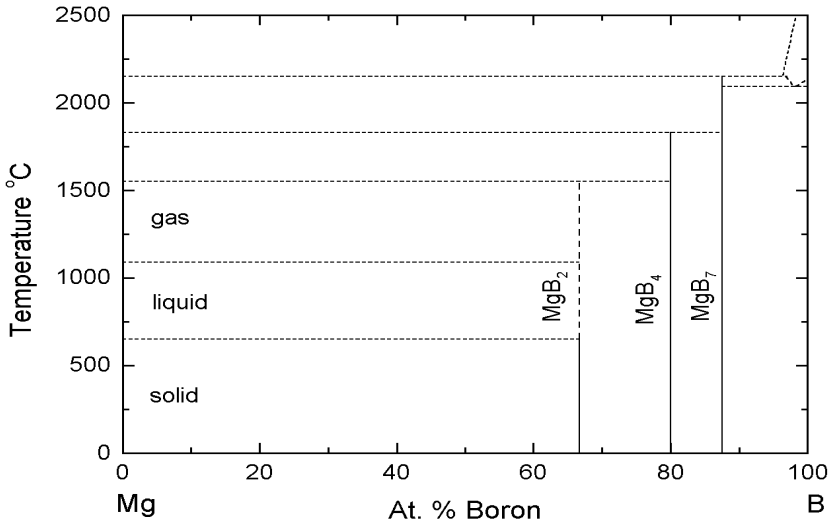

Fig. 1. Proposed binary phase diagram for the B-Mg system (after ref. [2]).

Indeed attempts to find exposed surfaces of primary solidification for MgB_2 in ternary and quaternary melts have, up to this point in time, failed. On the

other hand we have found that it is relatively simple to synthesize polycrystalline samples of MgB_2 by reacting boron powder (or filaments or films) with Mg vapor. The powder samples that will be discussed below have been synthesized as follows [3]: stoichiometric quantities of high purity Mg (99.99%) and isotopically pure boron (< 100 mesh, 99.5% from Eagle Picher) were sealed into a Ta tube under an atmosphere of high purity argon. The sealed Ta tube was itself sealed into a quartz ampoule and was placed into a box furnace that was at 950°C for a given time (usually two hours). The reaction ampoule was then quenched into cold water and the Ta tube was pealed away from the MgB_2 which, at this point, was in the form of a pellet.

Figure 2 presents a powder X-ray diffraction pattern of MgB_2 that has been produced in this manner. Figure 3 presents powder x-ray diffractions patterns from samples that have been reacted for various times ranging from 15 minutes to 4 hours. As can be seen by 2 hours the MgB_2 peaks are fully developed. For short times, t < 30 minutes, the MgB_2 peaks are not as well developed and we find extra peaks that are associated with unreacted Mg [4]. For carefully reacted samples with a stoichiometric ratio of Mg and B powder X-ray diffraction patterns can be found the have no extraneous peaks. Figure 4 is an electron microscope image of the grains in a pellet of MgB_2 made in this manner. As can be seen the pellet is made up of individual grains with linear dimensions between 0.5 – 5.0 μm.

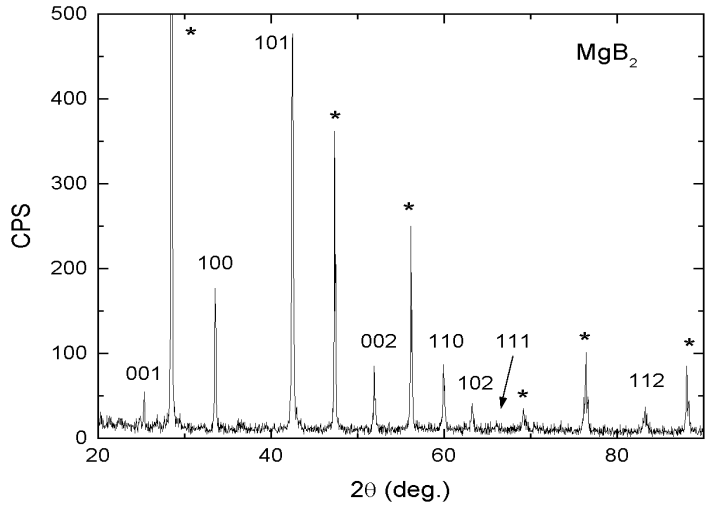

Fig. 2. Powder X-ray (Cu $K\alpha$ radiation) diffraction spectra of MgB_2 (with h, k, l values) and Si standard (*).

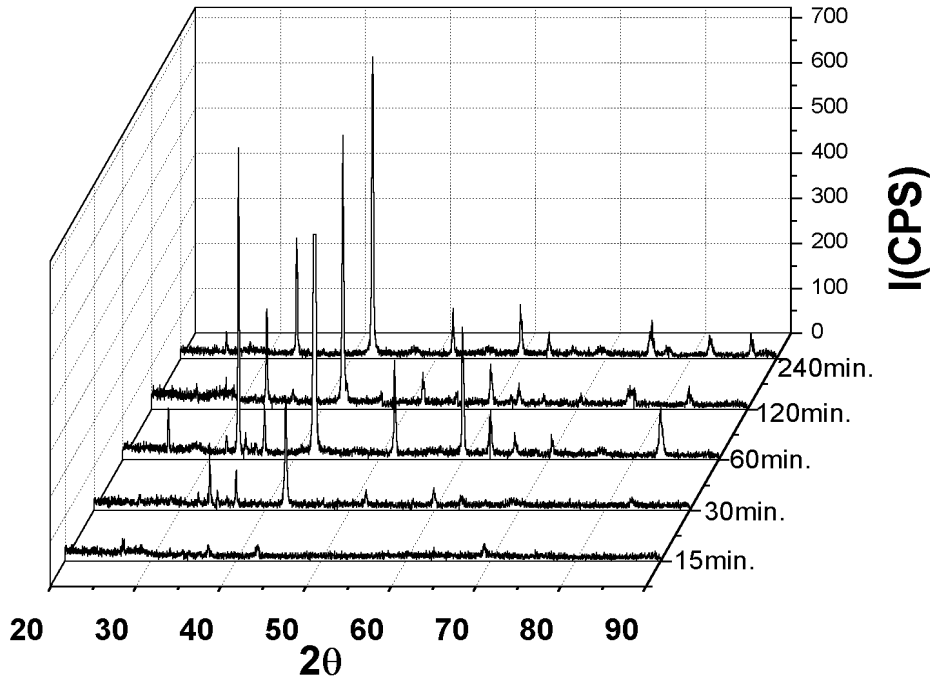

Fig. 3. Powder X-ray diffraction patterns from samples of MgB_2 that have been reacted at 950°C for representative times (as described in text) [4].

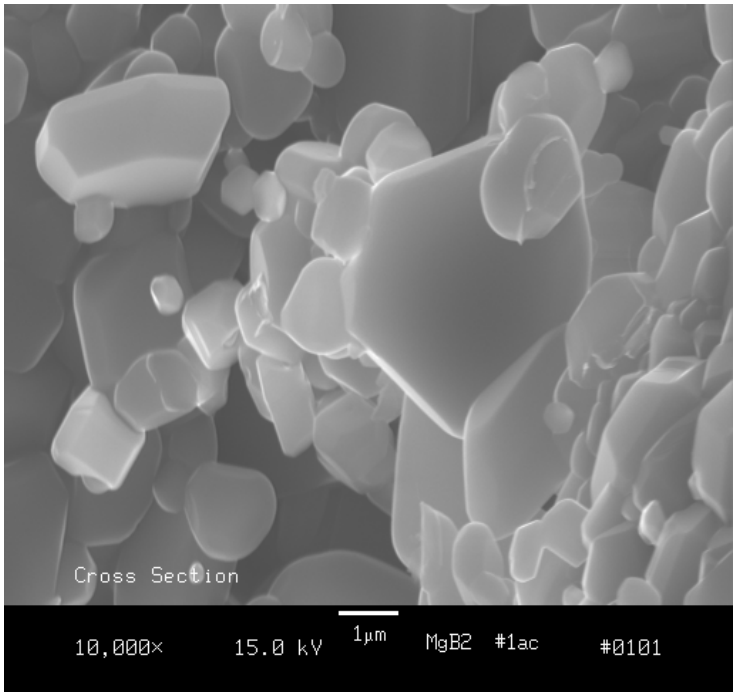

Fig. 4. Electron microscope image of the snapped surface of a MgB_2 pellet. Note: white horizontal bar is 1 µm.

MgB_2 can be formed in a variety of morphologies depending upon the form of the boron that is exposed to Mg vapor. Boron is available in the form of filaments that range in diameters from 100 – 300 μm [5,6]. Segments of dense MgB_2 wire can be synthesized by exposing such boron fibers to Mg vapor as follows [7]. Segments of boron filament are sealed into a Ta tube with excess Mg (often with a stochiometry close to Mg_2B). Given that MgB_2 is the most Mg-rich binary compound (see figure 1), an excess of Mg insures that there is adequate Mg in the reaction vessel to allow the complete transformation of the boron into MgB_2. The Ta tube is then sealed into quartz and placed in a furnace that is at 950°C and left to react for two or more hours (depending upon the size of the starting boron filament). Once the reaction is complete the ampoule is removed from the furnace and quenched to room temperature.

As an aside, one growth was performed specifically to demonstrate that the MgB_2 formed solely as a result of exposure to Mg *vapor*. In this case the boron filaments were segregated from the liquid Mg: i.e. placed a centimeter above the liquid Mg (via a series of crossed strainers). This well defined separation of the filaments from the liquid Mg made no difference in the final outcome. After two hours at 950°C the MgB_2 wires were well formed.

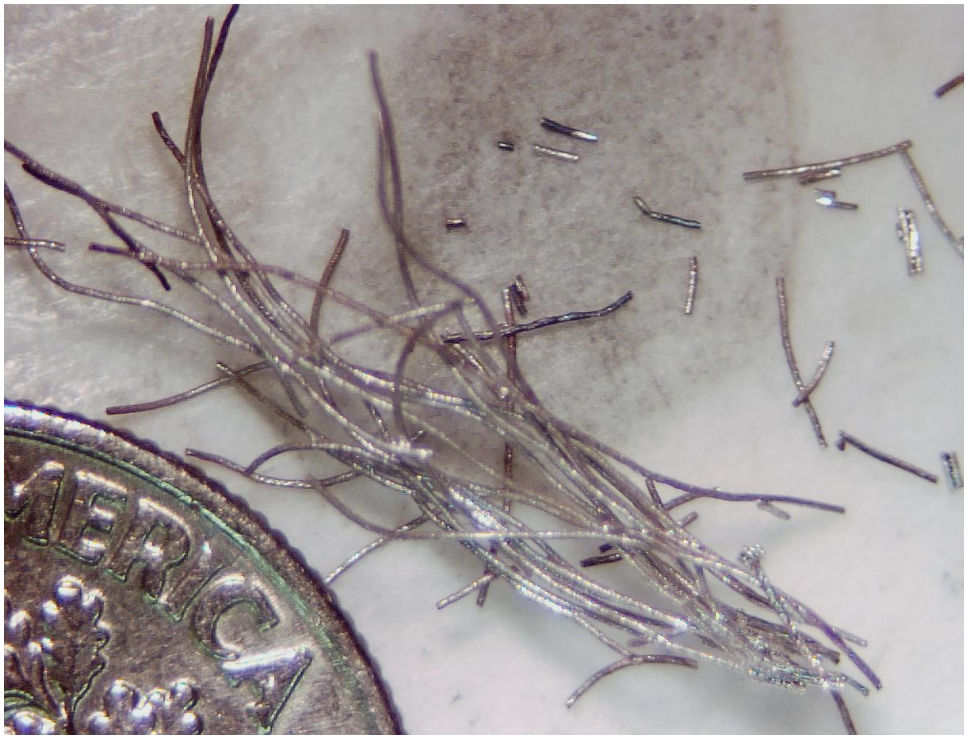

Fig. 5. MgB_2 wire segments made from 100 μm diameter boron filaments. Note: part of U. S. dime in lower left-hand corner for scale [7].

Figure 5 shows a picture of wire segments that were made from 100 μm boron filament that was reacted for 2 hours at 950°C. The segments are somewhat bent and distorted but are mechanically robust. The deformation very likely is associated with a dramatic increase in volume during the reactions. Figure 6 shows a snapped cross section of a 100 μm boron filament as well as the snapped cross section of the MgB_2 wire segment that resulted from the exposure to Mg vapor. The diameter of the MgB_2 wire is approximately 150 μm. Similar increases in size are observed in wire segments synthesized from 140, 200 and 300 μm boron filaments. The central feature seen in both the un-reacted filament as well as in the MgB_2 wire segment is a tungsten boride core that is approximately 15 μm in diameter and a result of the process that is used to synthesize the boron fiber [5]. As will be shown below there is no apparent contamination from the tungsten nor effect associated with having it in parallel with the MgB_2.

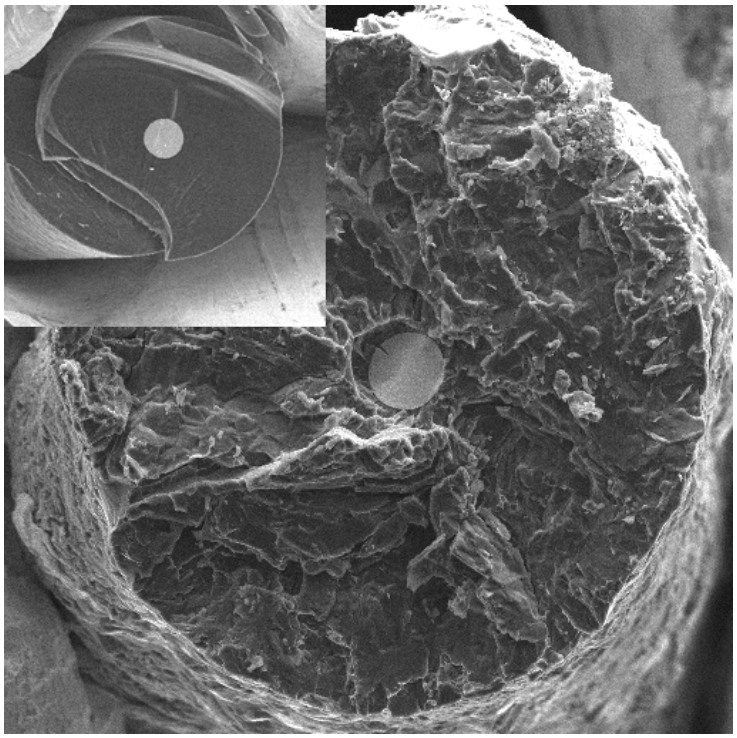

Fig. 6. Electron microscope image of a snap cross section of a ~160 μm MgB_2 wire. Inset: Image of the un-reacted 100 μm boron filament. Note: in both images a central core of tungsten boride (diameter ~ 15 μm) can be clearly seen [7].

Figure 7 is an optical microscopy image (using polarized light) of an ~200 μm diameter MgB_2 fiber synthesized from a 140 μm diameter fiber. The different colors come from the slightly different absorptions associated with the different alignment of the individual grains. In this image the

tungsten boride core is split. The density of the wire segments is estimated to be better than 90 % of the theoretical density.

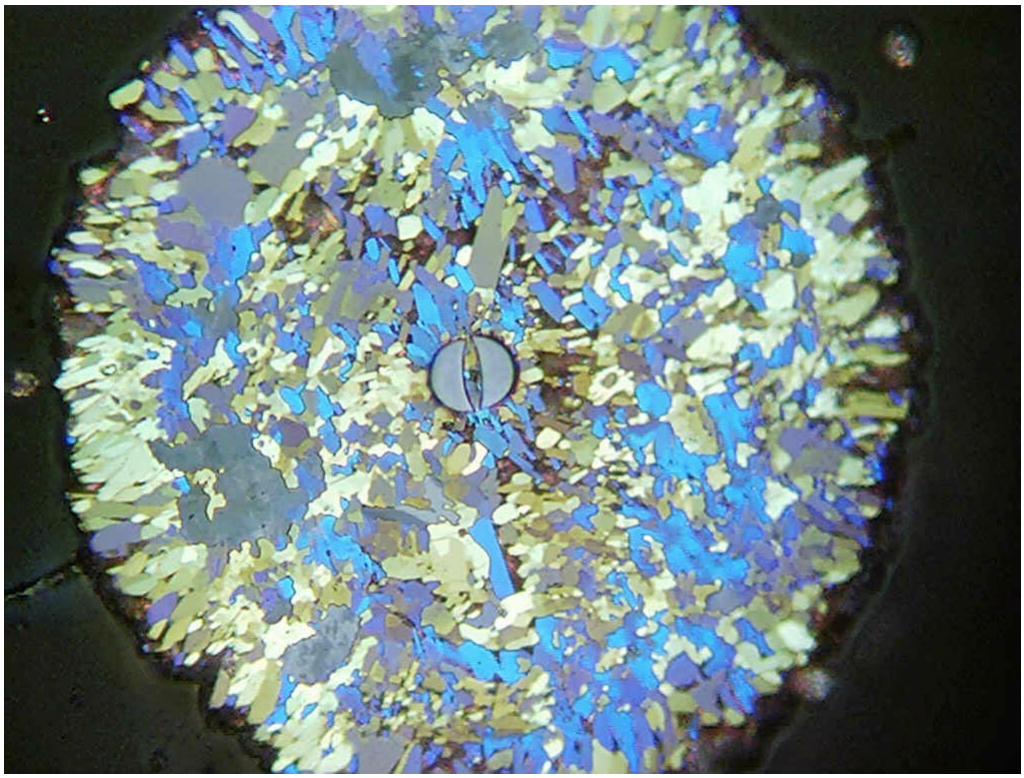

Fig. 7. Optical microscope image (using polarized light) of a polished cross section of ~ 200 μm diameter MgB_2 wire.

In addition to wires, MgB_2 can be produced in the form of thin films in a similar manner. As discussed in Ref [7], exposure of boron in differing morphologies (filaments, tapes, films) to Mg vapor can lead to superconducting MgB_2 with tailored form (wires, tapes, films). In specific, thin films of boron can be deposited onto substrates (such as $SrTiO_3$). These thin films of boron can then be reacted with Mg vapor in a manner similar to that described above for the wires, although much smaller reaction times will be needed given the much smaller thickness of the boron films. Films made in this manner have relatively high superconducting transitions (T_c = 39 K) [8]. This procedure for producing thin films of MgB2 has recently been used by other groups as well [9,10,11].

PHYSICAL PROPERTIES OF MgB_2

Polycrystalline samples of isotopically pure $Mg^{10}B_2$ and $Mg^{11}B_2$ were synthesized via a 2 hour reaction at 950°C. The temperature dependent

magnetization and resistance data from these samples near T_c are shown in figure 8. The resistive transition shows a shift in T_c of 1.0 K, with $T_c(Mg^{11}B_2)$ = 39.2 K and $T_c(Mg^{10}B_2)$ = 40.2 K, using an offset to define T_c. A similar shift in T_c is detected in the temperature dependent magnetization measurements. Using an onset criterion of 2% deviation from normal state, $T_c(Mg^{11}B_2)$ = 39.2 K and $T_c(Mg^{10}B_2)$ = 40.2 K. (The data were collected upon warming, after cooling to 5 K in zero applied field, and then applying a field of 25 Oe.) As discussed in reference [3], the shielding value exceeds $-1/4\pi$, but this is associated with the demagnetization factor. When a similar measurement is made on a dense sample of wire with a small, well defined demagnetization factor the shielding is very close to $-1/4\pi$ [7].

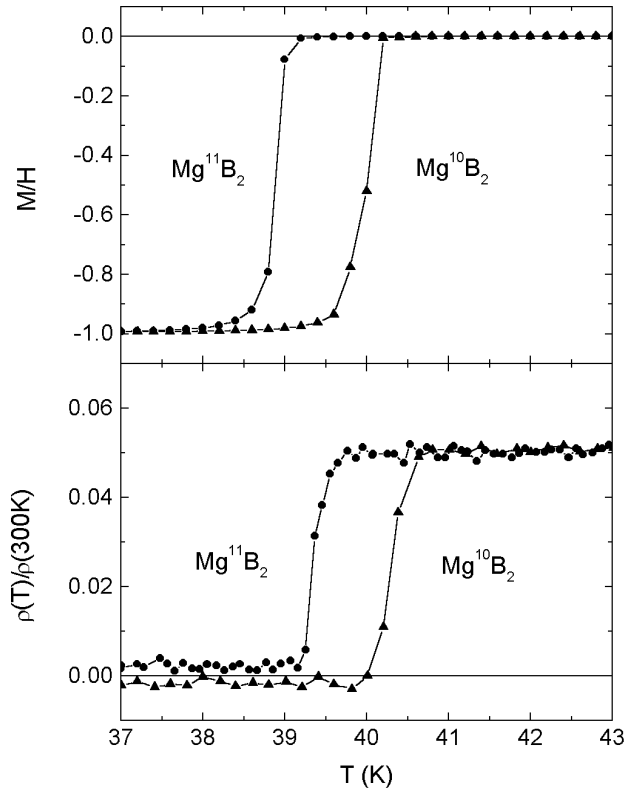

Fig. 8. Temperature dependent magnetization (upper panel) and resistivity (lower panel) of isotopically pure MgB_2 near T_c. Note: the magnetization data is normalized to –1 at low temperatures.

Figure 9 presents data on the specific heat of isotopically pure MgB_2 samples near T_c. These data also show an isotope shift of approximately 1 K. The superconducting transition temperatures determined from the low field

magnetization and resistivity data for each sample are indicated by the vertical arrows.

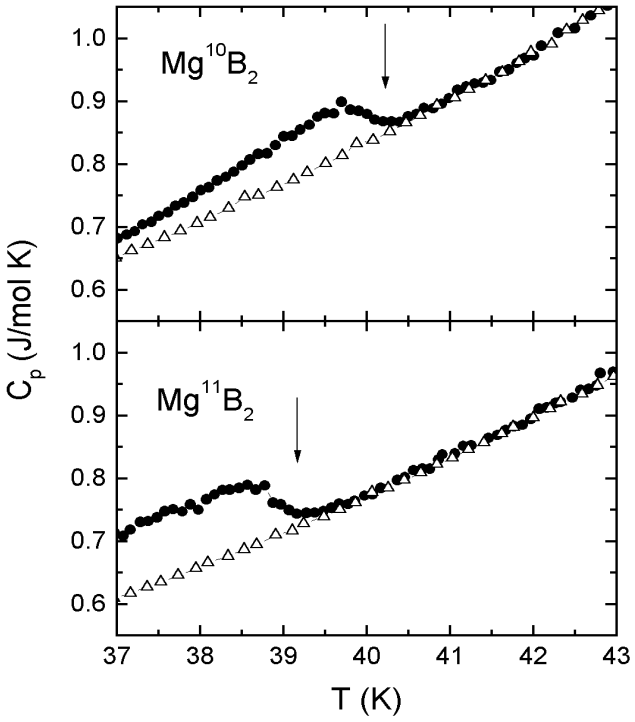

Fig. 9. Temperature dependence of specific heat near T_c for isotopically pure samples of MgB_2. Filled circles are data taken in zero applied magnetic field and open triangles are data taken in an applied field of 9 T. The vertical arrows indicate the T_c values taken from magnetization and resistivity data shown in figure 8 [3].

The shift in T_c associated with the boron isotope effect is delightfully large, fairly simple to measure and robust. Similar shifts in T_c have been subsequently measured on several different batches as well as by other groups [12,13]. In the simplest analysis, for a weak-coupled BCS superconductor, T_c would be inversely proportional with the square root of the formula unit mass. In this case the shift in T_c would be 0.87 K. On the other extreme, if superconductivity were due solely to boron vibrational modes, then T_c would be proportional to the inverse of the square root of the boron mass and a shift in T_c of up to 1.9 K could be possible. A shift in T_c of 1.0 K is then consistent with the phonons that mediate superconductivity being somewhat rich in boron nature.

More formally, we can estimate the partial (boron) isotope exponent α_B in this compound via $\alpha_B = - \Delta ln\ T_c / \Delta ln\ M_B$ [14,15]. From the measured values

of T_c, the boron isotope exponent can be estimated as $\alpha_B = 0.26 \pm 0.03$. It is worth mentioning that this value is close to the boron isotope exponents obtained for the YNi_2B_2C and $LuNi_2B_2C$ borocarbides, [16,17] where theoretical work [18] suggested that the phonons responsible for the superconductivity are high-frequency boron A_{1g} optical modes. Early band-structure calculations [19] suggested substantial electron transfer from the magnesium atom to the two boron atoms in the unit cell. Recent band structure works [20,21] suggests that the superconductivity in MgB_2 is essentially due to the metallic nature of the boron sheets. It should be noted that whereas the determination of a 1 K isotope shift in MgB_2 is not proof that MgB_2 is a phonon mediated BCS superconductor, it is certainly consistent with this conclusion.

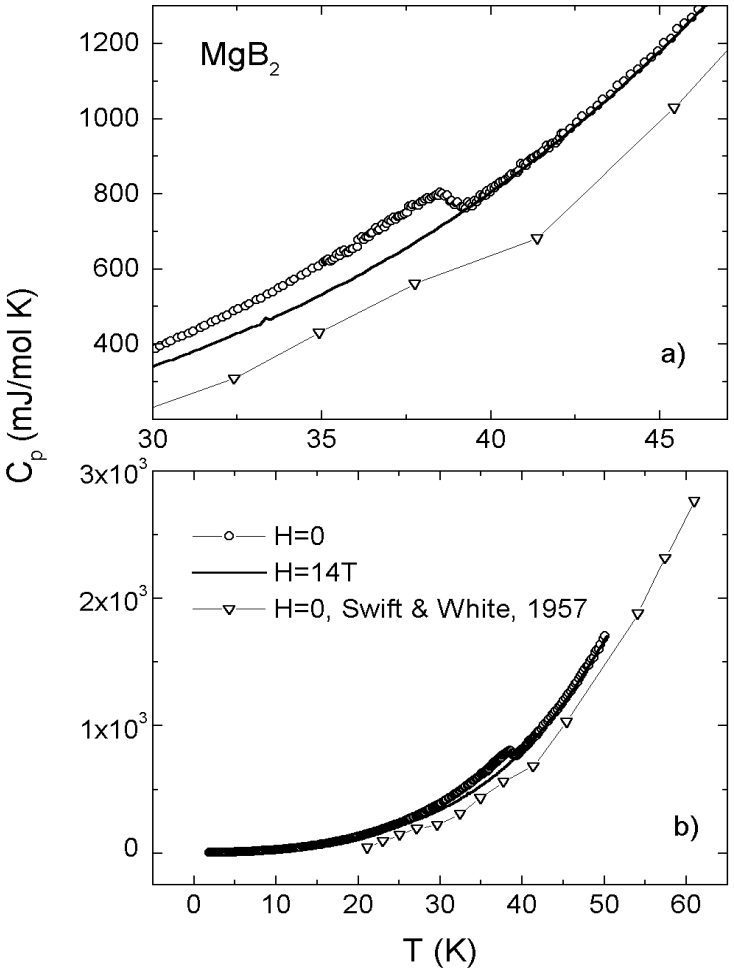

Fig. 10. Specific heat of $Mg^{11}B_2$ shown over (a) a temperature range near Tc and (b) an expanded temperature range. The open circles are data taken in zero applied magnetic field, the solid line is data taken in an applied field of 14 T and the open triangles are data taken from a table in Ref. [22].

Figure 10 presents the specific heat data of MgB2 over a wider temperature range. The open circles are data taken in zero applied magnetic field and the solid line is the loci of data in an applied field of 14 T. By fitting the high field data to a simple Debye model values of $\Theta_D = 775 \pm 30$ K and $\gamma_{el} = 2.4 \pm 0.5$ mJ/mol K^2 can be obtained. Whereas the value of Θ_D is similar to that reported in Ref. [3] the value of γ_{el} is more reliable due to the larger applied field of 14 T which allows us to measure the normal state to much lower temperatures (see figure 14 below). The value of Θ_D is quite high and is consistent with MgB_2 being a hard material with high characteristic phonon frequencies. Using the above values, and estimating a $\Delta C_p(T_c) = 92.6$ mJ/mol K from figure 10a, we get a value of $\Delta C_p/\gamma_{el}\ T_c \sim 1$. A more refined value of $\Delta C_p/\gamma_{el}\ T_c$ can be obtained if better values of ΔC_p and γ_{el} can be extracted from the data. Whereas a more refined value of ΔC_p can be obtained by using equal entropy constructions etc. this makes relatively little sense given the size of the error bars associated with the value of γ_{el}. More refined values of γ_{el} will have to wait for measurements of C_p in field in excess of $H_{c2}(0)$ (~ 17 T as shown below). Figure 10 also shows $C_p(T)$ data for MgB_2 that was presented in tabular form in 1957 by Swift and White [22]. These data agree fairly well with our data set in the region of overlap. Swift and White failed to detect the superconducting phase transition near 40 K and fit the temperature dependence of their data to a power law in T from 20 to 80 K. This is a reasonable treatment of their data, but one has to wonder how the history of superconductivity would have been changed if superconductivity in MgB_2 near 40 K had been discovered in the 1950's.

Having addressed the question of mechanism (to some extent at least), the next basic question is what are the basic properties of MgB_2? The temperature dependent resistivity of MgB_2 wire is shown in figure 11. In addition the resistance of a piece of sintered pellet of MgB_2 is shown in Fig. 12. In both cases the residual resistivity ratio (ρ(300 K)/ρ(42 K)) is large, ~20 for the pellet and ~25 for the wire. In the case of the wire sample the geometry and density are much better defined and the resistivity can be accurately determined: ρ(300 K) = 9.6 μOhm-cm and ρ(40 K) = 0.38 μOhm-cm. The resistivity of the pellet can be estimated. Based on the geometry of the sample the resistivity at 42 K is roughly 1 μOhm-cm, this is higher than the resistivity of the wire sample; a deviation that is consistent with the lower density of the sample leading to a falsely high value of resistivity.

It should be noted that the temperature dependencies of the resistance (resistivity) for both the sintered pellet and the wire samples are virtually

identical. This simple observation is important since it supports the assumption that the resistivity that we are measuring is intrinsic to MgB_2 and not some artifact associated with the synthesis of the wire, e.g. tungsten boride core or Mg on the surface. The temperature dependent resistivity (resistance) shown in figures 11, 12 can be fit by a power law $\rho = \rho_0 + \rho_1 T^{\alpha}$ with $\alpha \approx 2.6 - 2.8$ between T_c and 200 K [6,23]. Description of the normal state resistivity in the whole available temperature range (up to 300 K) with Bloch – Grüneisen expression [24] is in a very good agreement with the experiment.

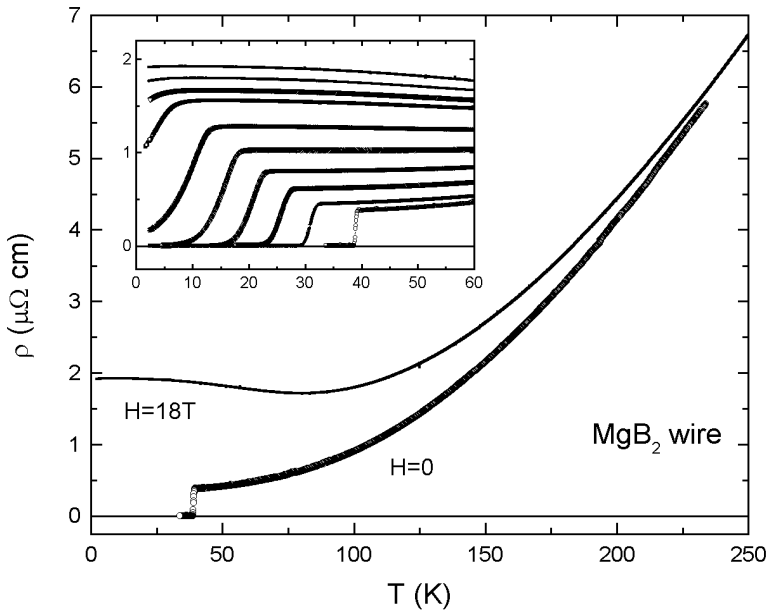

Fig. 11. Temperature dependent electrical resistivity of MgB_2 wire in zero applied magnetic field and an applied field of 18 T. Inset: lower temperature resistivity of MgB_2 wire for applied magnetic fields of 0, 2.5, 5, 7.5, 10, 12.5, 15, 16, 17 and 18 T [26].

MgB_2 has a remarkably low, normal state resistivity. The value of $\rho(42\ K) = 0.38\ \mu$Ohm-cm is comparable to that of copper wire and over a factor of 20 times lower than that of polycrystalline Nb_3Sn [7]. This by itself is a very important property of MgB_2 and promises to be of considerable use. For example it means that in the normal state MgB_2 can carry substantially higher current densities than other superconductors with less Joule heating. On the other hand though, such low resistivity values are not unusual for boron rich materials and this low resistivity by itself does not make MgB_2 anomalous. It

is the combination of a high T_c *and* a low normal state resistivity that makes MgB_2 particularly appealing.

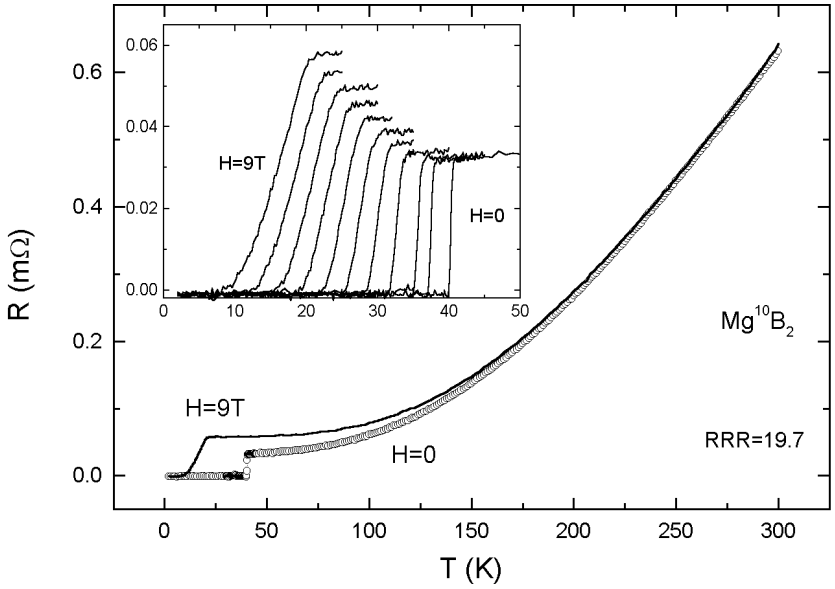

Fig. 12. Temperature dependent electrical resistance of $Mg^{10}B_2$ pellet in zero and 9 T applied magnetic field. Inset: lower temperature resistivity of $Mg^{10}B_2$ pellet for applied magnetic fields of 0, 0.5, 1, 2, 3, 4, 5, 6, 7, 8, and 9T [23].

Figures 11 and 12 also present the temperature dependent resistivity (resistance) of MgB_2 under applied magnetic fields. As can be seen there is a substantial magneto-resistivity at low temperatures. These data can be plotted on a Kohler's plot, figure 13, which reveals that $\Delta\rho/\rho_0$ is a simple power law of H/ρ_0 over most of the field / temperature range. This implies that there is a single salient scattering time in the normal state and is consistent with MgB_2 being a relatively simple intermetallic compound. It should be noted that since such magneto-resistance requires a small ρ_0 in order to be seen, measurements on samples that have large residual resistivities [25] will not display this behavior (extrinsic scattering will hide this intrinsic effect).

In addition to delineating the normal state properties, the temperature and applied magnetic field dependence of the resistivity provides information about the $H_{c2}(T)$ curve. T_c can be determined from the temperature dependence of the resistivity by using onset, maximum derivative or offset criteria. The onset criterion takes T_c to be the temperature at which linear

extrapolation of ρ(T) at the superconducting transition intersects the extrapolation of the normal state ρ(T) to lower temperatures, the maximum derivative criterion takes T_c to be the temperature of the maximum in dρ/dT, and the offset criterion takes T_c to be the temperature at which linear extrapolation of ρ(T) at the superconducting transition intersects ρ = 0 line. All three data points are plotted in figure 14 for selected values of applied field using a sample of MgB_2 wire [26]. Similar data was obtained on a $Mg^{10}B_2$ sintered pellet and is shown in figure 15 along with other critical field data derived from magnetization measurements discussed below. It should be noted that the temperature dependence of $H_{c2}(T)$ is rather curious and bears a striking resemblance to that found for YNi_2B_2C and $LuNi_2B_2C$: a large, linear in temperature range with slight upward and downward curvatures near T_c and 0 K respectively. [7,23,27-29].

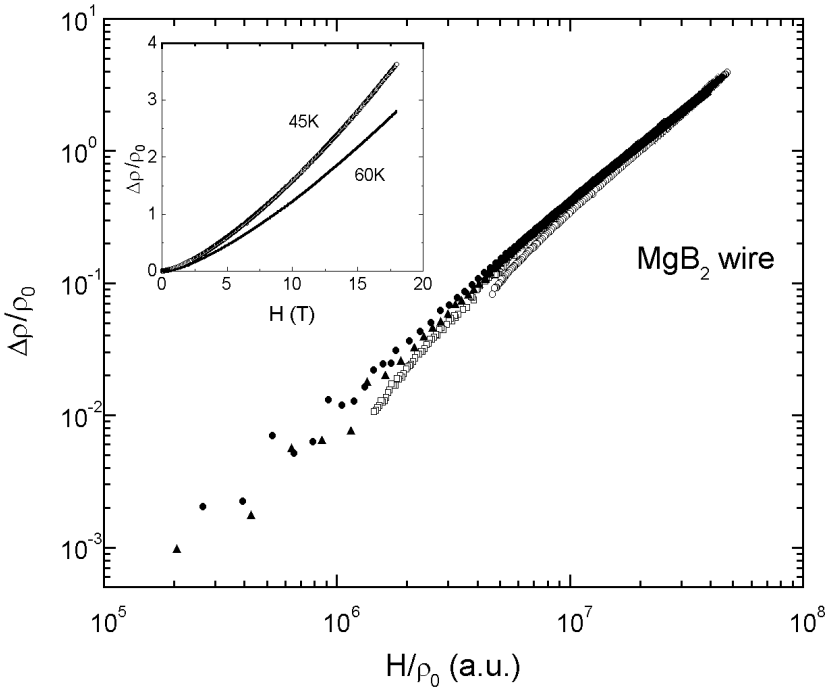

Fig. 13. Kohler's plot for MgB_2 wires: open symbols from ρ(T) at different applied fields, filled symbols from ρ(H) at 45 and 60 K. Inset: $\Delta\rho(H)/\rho_0$ at 45 and 60 K [26].

Figure 16 presents magnetization loops for MgB_2 at representative temperatures and the inset of figure 16 shows similar loops taken over a wider range of temperatures and fields. The magnetization data are reversible (to within ~1%) for higher fields and then suddenly depart from reversibility for

fields below H_{irr} (shown for 30 and 36 K). Given the small, normal state magnetization of MgB_2, $H_{c2}(T)$ and H_{irr} can be easily determined from these data and are plotted in figure 15. As can be seen there is good agreement between the values of $H_{c2}(T)$ determined from the magnetization and the value determined from the resistivity data and the onset criterion. It should be noted that the irreversibility line (figure 15) that is determined from the magnetization loops presented in figure 16 is in good agreement with the irreversibility line inferred from NMR data on similar $Mg^{11}B_2$ samples [30].

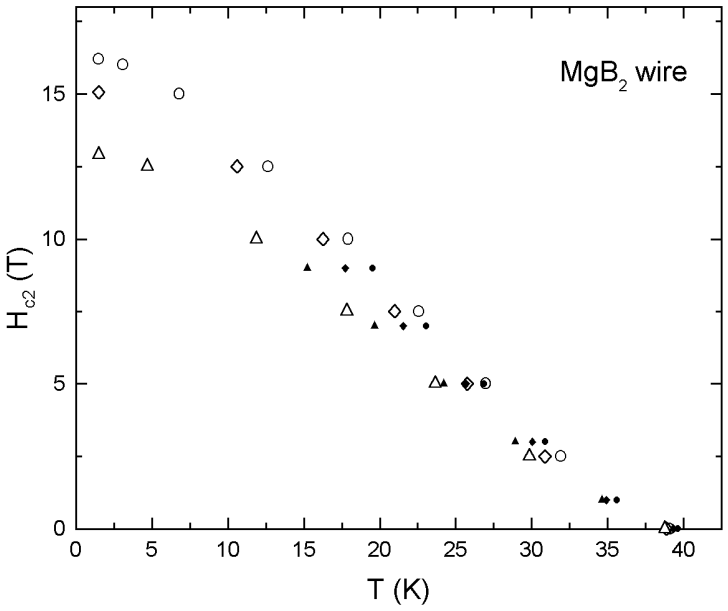

Fig. 14. Upper critical field for MgB_2 wire. Values were extracted from magneto-transport measurements similar to that shown in figure 11. For each applied field value onset, maximum slope and offset temperature values are plotted [26].

The critical current density can be inferred from the magnetization loops via the Bean model [23]. Figure 17a presents the $J_c(H)$ values for selected temperatures that have been extracted from the M(H) loops shown in figure 16. Given that the sample used was a piece of sintered pellet the dimension of the sample used in the Bean equation was the diameter of the equivalent sphere, d ~ 1 mm. Similar data were taken on a segment of MgB_2 wire and are shown in figure 17b. In this case both M(H) loops as well as direct measurement of V(I) were used to determine the critical current density. The maximum value of J_c for the wire samples is roughly a factor of 3 higher than that found for the sintered pellet. In addition the low current density values of

J_c (that were directly measured from V(I) curves) are substantially higher than the values inferred from the Bean model and the M(H) loops. To at least some extent this is associated with the fact that for low J_c values the Bean model becomes statistically more inaccurate due to the increasing reversibility of the M(H) loops.

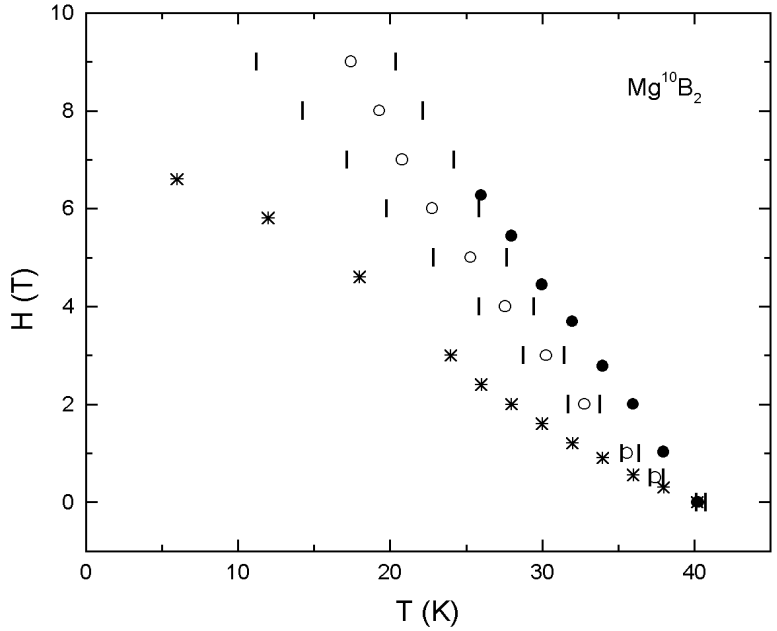

Fig. 15. Upper critical field of $Mg^{10}B_2$ determined resistively (onset and offset are vertical bars and maximum slope are open circles) and from magnetization data (filled circles). Asterisks show H_{irr} [23].

One other parameter that can be extracted from the M(H) curves is an estimate of the thermodynamic critical field H_c. This is achieved by first assuming that the same pinning force will exist for increasing and decreasing applied magnetic fields and then finding the area under the average magnetization, $M_{ave} = ½ (M_{up} + M_{down})$, curve. [23,31]. Plots of the critical field for the sintered pellet is shown in Fig. 18. It should be noted that the slope of the $H_c(T)$ plot is related to the jump in the specific heat at T_c by $\Delta C = [VT_c/4\pi][dH_c/dT]^2$. Using $dH_c/dT = 120$ Oe/K this gives $\Delta C = 80$ mJ/mole K, a value that is close to $\Delta C = 92.6$ mJ/mol K found from the data in figure 10.

Using the data presented above values of several salient length scales can be determined. The electronic mean free path at 42 K can be estimated to be $l \sim 60$ nm by taking the residual resistivity, calculated Fermi velocity, $v_F \sim$

4.8 10^7 cm/s, and an estimate of the carrier density, 6.7 e/cm^3, based on the simple assumption of two free electrons per unit cell [7].

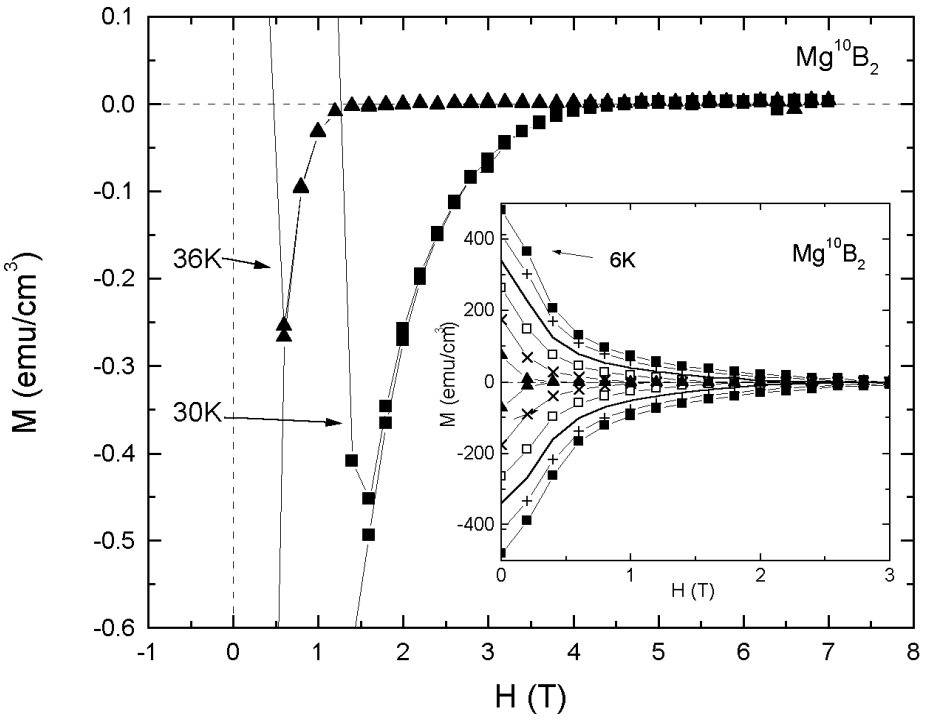

Fig. 16. Expanded view of magnetization loops on pellet of $Mg^{10}B_2$ for T = 30 and 36 K. Inset: magnetization loops over larger M-H range for T = 6, 12, 18, 24, 30, 36 K [23].

This can be compared to the superconducting coherence length ξ_0 which can be determined from the low temperature limit of H_{c2} by using: $\xi_0 = [\phi_0/2\pi H_{c2}]^{1/2}$. Using $H_{c2}(0\ K) \sim 16$ T from figure 14, $\xi_0 \sim 4.4$ nm. Given that $\xi_0 << l$, MgB_2 is deeply in the clean limit. The Ginsburg-Landau parameter can be determined by using, $\kappa = H_{c2}/\sqrt{2}\ H_c \sim 30$ for the sintered $Mg^{10}B_2$ sample. Using this value of κ the London penetration depth, λ can be found to be ~ 132 nm by using $\kappa = \lambda/\xi_0$.

It is important to note that whereas the values given above are simply estimates of l, ξ_0 and λ, two conclusions are unambiguous: the MgB_2 samples are deep within the clean limit ($l/\xi_0 >> 1$) and are extreme examples of type-II superconductors ($\kappa >> 1$).

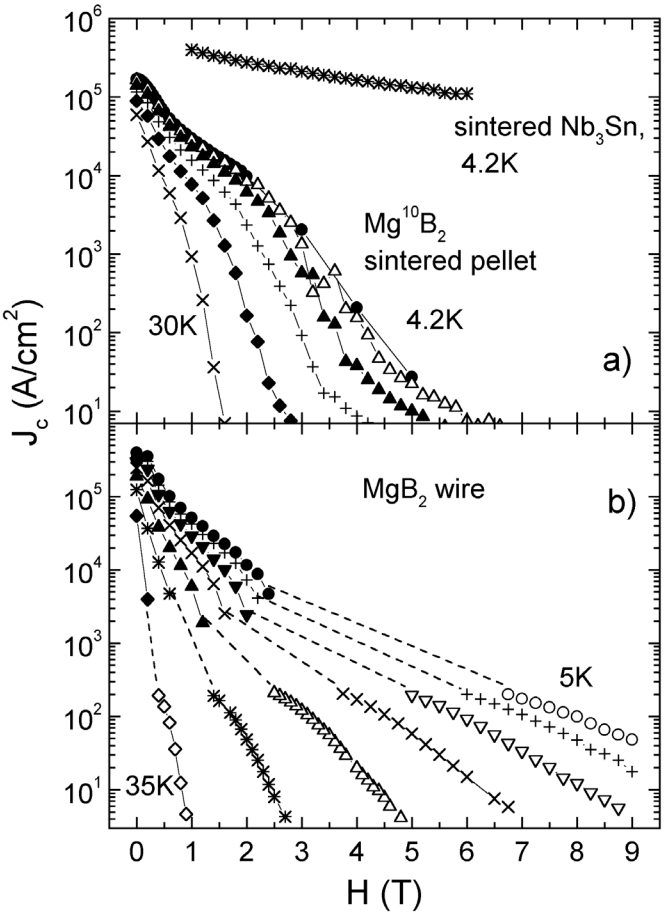

Fig. 17. Superconducting critical current density of (a) $Mg^{10}B_2$ sintered pellet and (b) ~150 μm diameter wire. It should be noted that for the wire sample the lower current density (open symbol) data points were taken from V(I) data. All other data points have been inferred from M(H) data via the Bean model [7,23].

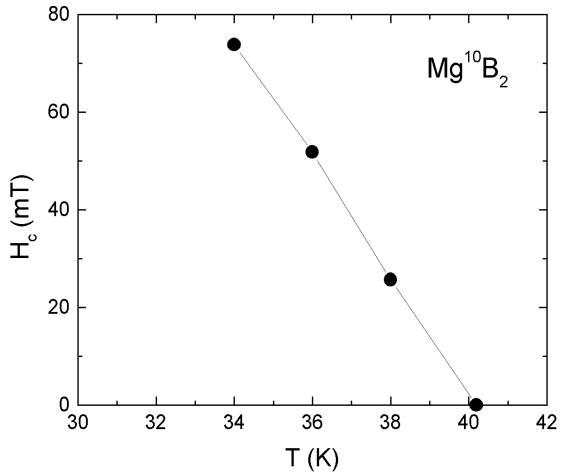

Fig. 18. Critical field H_c for sintered $Mg^{10}B_2$ pellet [23].

Up to this point the analysis of the data has implicitly assumed a relatively isotropic superconducting groundstate. Recent measurements of conduction electron spin resonance (CESR) as well as magnetization indicate that MgB_2 may actually have a highly anisotropic $H_{c2}(T)$ [32]. An anisotropyas large as 6-9 can be inferred from magnetization measurements. For a sample that consists of randomly oriented grains of a uniaxial superconductor with the anisotropy $\gamma = H_{c2}^{ab}/H_{c2}^{c}$ placed in a field H along z - axis the magnetization can be written (for the case of $\gamma > 1$) as

$$M_z = - M_0 f(H),\ M_0 = \phi_0/[32\pi^2\lambda^2\beta\gamma^{1/3}(\gamma^2-1)^{1/2}] \qquad (1)$$

$$f(h) = (1-4h^2)/3h^2\ (1-h^2)^{1/2} + ln\ \{[1+(1-h^2)^{1/2}]/h\} \qquad (2)$$

where $\beta = 1.16$, $h = H/H_{c2}^{ab}$, $\lambda = (\lambda_{ab}^2\lambda_c)^{1/3}$, and ϕ_0 is a flux quantum (here we skip derivation and important discussions related to these equations and refer thoughtful reader to [32-34]). Figure 19 shows the reversible part of the field dependent magnetization M(H) for a number of temperatures together with solid curves obtained by fitting the data to the equations above. The prefactor $M_0(T)$ and the in-plane upper critical field $H_{c2}^{ab}(T)$ were taken as fitting parameters. The resulting values of both these parameters re reasonable and

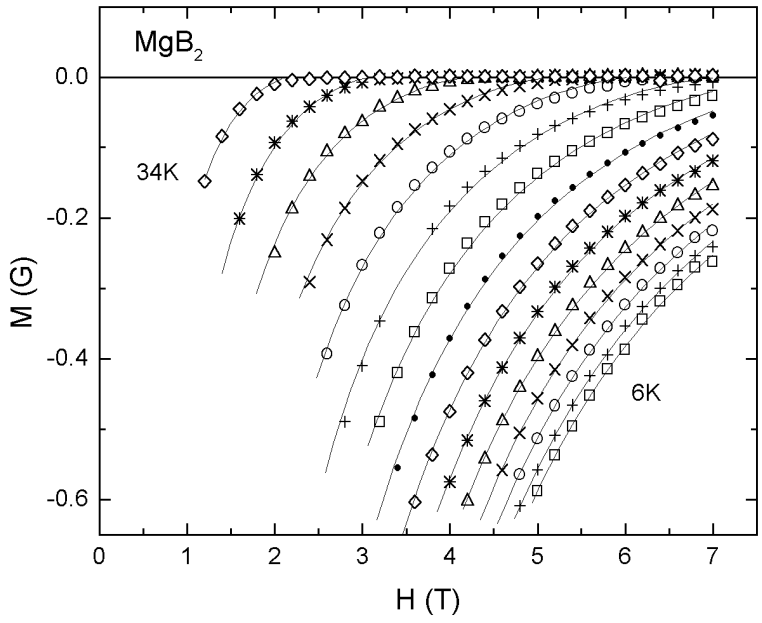

Fig. 19. Reversible magnetization M(H) of MgB_2 at temperatures from 6 K to 34 K with a 2 K step. Solid lines are calculated with the help of equations (1), (2) [32].

their temperature dependencies behave as expected. The fits give the limiting value $M_0(T\rightarrow 0) \approx 0.26$ G that translates to $\lambda^2(0)\gamma^{1/3}(\gamma^2-1)^{1/2} \approx 2.1\ 10^{-9}$ cm^2. Estimates of $\lambda(0)$ range between 110 nm [35] and 140 nm [23], which yield the anisotropy of the upper critical field $\gamma \approx 6$-9.

Independently, the H_{c2} anisotropy can be evaluated from the broadening of the resistive transition in an applied magnetic field. The theoretical approach was developed more than a decade ago and used for $YBa_2Cu_3O_{7-x}$ [36]. It is based on the anisotropic Ginzburg – Landau theory of the upper critical field and the Davidson – Tinkham phenomenological

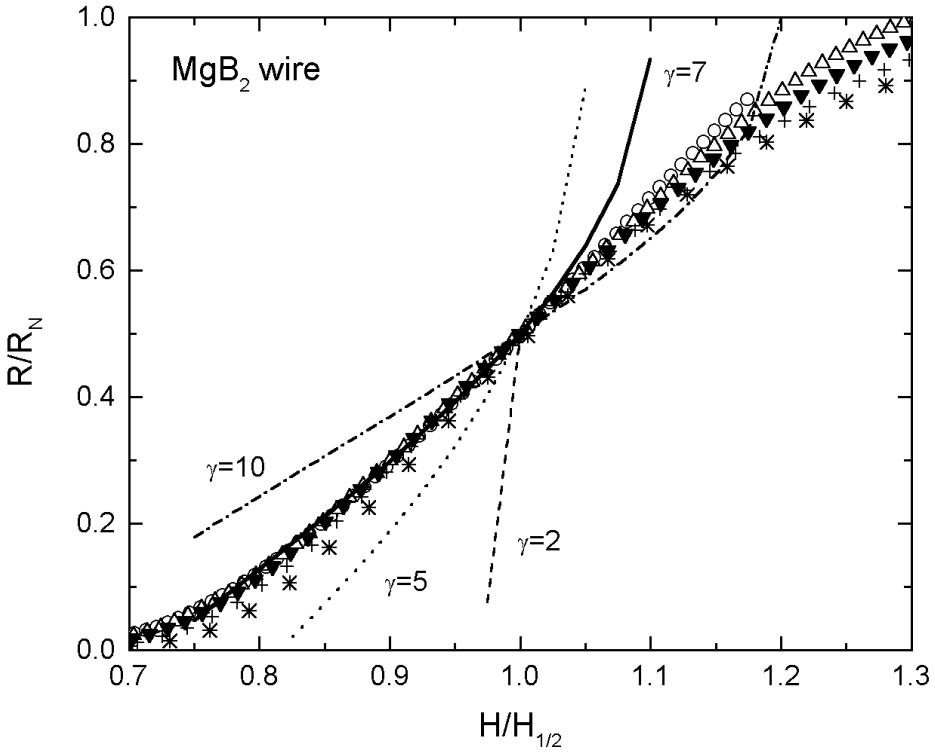

Fig. 20. Magnetic field dependence of the resistance of MgB_2 wires at 22.5, 25, 27.5, 30, and 32.5 K scaled by R_N and $H_{1/2}$ (see text). Lines are theoretical curves calculated using equations (3), (4).

equation for the resistivity of a heterogeneous aggregate of superconducting and normal crystallites [37]. Without going into details that can be procured from [36,37], the resistivity in a field H, $\rho(H)$, normalized to the normal state resistivity ρ_N can be written as

$$\rho(H)/\rho_N = (1-6f_s(H))(1+f_s(H)/X) \quad (3)$$

$$f_s(H) = \{[(H_{c2}{}^{max}/H)^2-1]/(\gamma^2-1)\}^{1/2} \quad (4)$$

where X, depolarization factor, depends on the crystallite shape [37], being X = 1/3 for spheres.

Figure 20 shows the field dependent resistance of MgB_2 wires through the superconducting transition at several temperatures. The resistance is scaled by the normal state resistance R_N, and the applied field is scaled by the field $H_{1/2}$ (the applied field for which the resistance reaches 0.5 R_N at that temperature). Lines present the behavior expected from the model mentioned above for several values of H_{c2} anisotropy γ. Figure 20 shows that $\gamma \approx 6$-9 can consistently describe magneto-transport data. It has to be mentioned that the estimates of γ from the broadening of the superconducting transition are somewhat less straightforward since an additional assumption about percolation is required and H_{c2} anisotropy is considered as the only mechanism for broadening, neglecting, for example, possible effects of fluctuations. On the other hand, the agreement between the magnetization and the magneto-transport-based estimates of gamma is encouraging.

A similar anisotropy can be inferred from CESR measurements [32] as well as analysis of M(T) at constant H data [38]. This later technique has also been used to find anisotropies in $H_{c2}(T)$ of powdered samples of Y1221 and Lu1221 which agree with single crystal data taken on samples from the same batches. Further research into the origin and implications of this and other [39] anisotropies is ongoing.

SUMMARY

The first half of 2001 has brought with it the discovery and characterization of a simple, intermetallic superconductor, MgB_2, that has a remarkably high $T_c \sim 40$ K. Even after just six months of research MgB_2 appears to be an exceptionally interesting material for basic as well as applied research. MgB_2 can be synthesized in the form of wires, tapes or films by exposing the appropriate form of boron (filament, tape, or thin film) to Mg vapor for the appropriate time (which depends upon the dimension of the boron used). This has lead to high-density samples of wires as well as thin films. In the normal state MgB_2 appears to be a relatively simple metal with one salient scattering time. In addition, MgB_2 has a large Θ_D, and, not unrelated, a low normal state resistivity. The superconducting transition

temperature of MgB_2 manifests a substantial boron isotope shift, a result that is consistent with MgB_2 being a phonon mediated, BCS superconductor. The $H_{c2}(T)$ measured on polycrystalline MgB_2 samples is linear in T over a wide range of effective temperature with $H_{c2}(0) \sim 16$ T. MgB2 appears to be an extremely type II superconductor with $\kappa >> 1$ and deep within the clean limit with $l >> \xi_0$. The superconducting critical current density of MgB_2 wires is 4 10^5 A/cm^2 at 5 K as inferred from the Bean model and there is every likelihood that this value can be increased by the addition of pinning mechanism.

ACKNOWLEDGEMENTS

Ames Laboratory is operated for the U. S. Department of Energy by Iowa State University under Contract No. W-7405-Eng.-82. This work was supported by the director for Energy Research, Office of Basic Energy Sciences.

REFERENCES

[1] J. Akimitsu, Symposium on Transition Metal Oxides, Sendai, 10 January 2001; J. Nagamatsu, N. Nakagawa, T. Muranaka, Y. Zenitani, and J. Akimitsu, Nature, **410** (2001) 63.

[2] *Binary Alloy Phase Diagrams*, edited by T. Massalski (A.S.M. International, Materials Park, OH, 1990), 2nd ed.

[3] S. L. Bud'ko, G. Lapertot, C. Petrovic, C. E. Cunningham, N. Anderson, and P. C. Canfield, Phys. Rev. Lett., **86** (2001) 1877.

[4] in: C. E. Cunningham, C. Petrovic, G. Lapertot, S. L. Bud'ko, F. Laabs, W. Straszheim, D. K. Finnemore, and P. C. Canfield, Physica C, **353** (2001) 5 these extra peaks were mislabeled as unreacted boron peaks.

[5] Textron Systems, 201 Lowell St., Wilmington, MA 01887, USA.

[6] Goodfellow Corp., 800 Lancaster Ave. Berwyn, PA 19312, USA.

[7] P. C. Canfield, D. K. Finnemore, S. L. Bud'ko, J. E. Ostenson, G. Lapertot, C. E. Cunningham, and C. Petrovic, Phys. Rev. Lett., 86 (2001) 2423.

[8] S. R. Shinde, S. B. Ogale, R. L. Greene, T. Venkatesan, P. C. Canfield, S. L. Bud'ko, C. E. Cunningham, and C. Petrovic, cond-mat/0103542, Appl. Phys. Lett. (2001) in press.

[9] W. N. Kang, H – J. Kim, E – M. Choi, C. U. Jung, and S – I. Lee, Science, **292** (2001) 1521.

[10] S. H. Moon, J. H. Yun, H. N. Lee, J. I. Kye, H. G. Kim, W. Chung, and B. Oh, cond-mat/0104230.
[11] S. F. Wang, S. Y. Dai, Y. L. Zhou, Z, H, Chen, D. F. Cui, J. D. Yu, M. He, H. B. Lu, and G. Z. Yang, cond-mat/0104555.
[12] D. G. Hinks, H. Claus, and J. D. Jorgensen, Nature, **411** (2001) 457.
[13] D. D. Lawrie, J. P. Franck, G. Zhang, C. Marcenat, and A. Pautrat, APS March Meeting, Seattle (2001).
[14] J. P. Franck, in *Physical Properties of High Temperature Superconductors IV*, edited by D. M. Ginsberg (World Scientific, Singapore, 1994), p.189.
[15] R. Kishore, in *Studies of High Temperature Superconductors*, edited by A. Narlikar (Nova Science Publishers, Commack, NY, 1999), vol. 29, p. 23.
[16] D. D. Lawrie and J. P. Franck, Physica C, **245** (1995) 159.
[17] K. O. Cheon, I. R. Fisher, and P. C. Canfield, Physica C, **312** (1999) 35.
[18] L. F. Mattheiss, T. Siegrist, and R. J. Cava, Solid State Commun., **91** (1994) 587.
[19] D. R. Armstrong and P. G. Perkins, J. Chem. Soc. Faraday Trans. 2, **75** (1979) 12.
[20] J. Kortus, I. I. Mazin, K. D. Belashchenko, V. P. Antropov, and L. L. Boyer, Phys. Rev. Lett., **86** (2001) 4656.
[21] J. M. An and W. E. Pickett, Phys. Rev. Lett., **86** (2001) 4366.
[22] R. M. Swift and D. White, J. Amer. Chem. Soc., **79** (1957) 3641.
[23] D. K. Finnemore, J. E. Ostenson, S. L. Bud'ko, G. Lapertot, and P. C. Canfield, Phys. Rev. Lett., **86** (2001) 2420.
[24] Y. Kong, O. V. Dolgov, O. Jepsen, and O. K. Andersen, Phys. Rev. B, **64** (2001) 020501(R).
[25] C. U. Jung, M – S. Park, W. N. Kang, M – S. Kim, S. Y. Lee, and S – I. Lee, Physica C, **353** (2001) 162.
[26] S. L. Bud'ko, C. Petrovic, G. Lapertot, C. E. Cunningham, P. C. Canfield, M – H. Jung, and A. H. Lacerda, Phys. Rev. B, **63** (2001) 220503(R).
[27] K. D. D. Rathnayaka, A. K. Bhatnagar, A. Parasiris, D. G. Naugle, P. C. Canfield, and B. K. Cho, Phys. Rev. B, **55** (1997) 8506.
[28] V. Metlushko, U. Welp, A. Koshelev, I. Aranson, G. W. Crabtree, and P. C. Canfield, Phys. Rev. Lett., **79** (1997) 1738.
[29] S. V. Shulga, S – L. Drechsler, G. Fuchs, K – H. Müller, K. Winzer, M. Heinecke, and K. Krug, Phys. Rev. Lett., **80** (1998) 1738.

[30] J. K. Jung, S. H. Baek, F. Borsa, S. L. Bud'ko, G. Lapertot, and P. C. Canfield, Phys. Rev. B, **64** (2001) 012514.
[31] M. Willemin, C. Rossel, J. Hofer, H. Keller, A. Erb, and E. Walker, Phys. Rev. B, **58** (1998) R5940.
[32] F. Simon, A. Janossy, T. Feher, F. Muranyi, S. Garaj, L. Forro, C. Petrovic, S. L. Bud'ko, G. Lapertot, V. G. Kogan, and P. C. Canfield, cond-mat/0104557, Phys. Rev. Lett. (2001) in press.
[33] V. G. Kogan and J. R. Clem, Jap. J. Appl. Phys., **26** (1987) 1159.
[34] V. G. Kogan and J. R. Clem, Phys. Rev. B, **24** (1981) 2497.
[35] J. R. Thompson, M. Paranthaman, D. K. Christen, K. D. Sorge, H. J. Kim, and J. G. Ossandon, Supercond. Sci. Technol., **14** (2001) L19.
[36] D. O. Welch, M. Suenaga, and T. Asano, Phys. Rev. B, **36** (1987) 2930.
[37] A. Davidson and M. Tinkham, Phys. Rev. B, **13** (1976) 3261.
[38] S. L. Bud'ko, V. G. Kogan, and P. C. Canfield, unpublished.
[39] I. C. McManus, Nature, **259** (1976) 426.